Proton Mobility in the In-Doped $CaZrO_3$ Perovskite Oxide

Ante Bilić* and Julian D. Gale

Nanochemistry Research Institute, School of Applied Chemistry, Curtin University of Technology, P.O. Box U1987, Perth 6845 WA, Australia

Received January 31, 2007. Revised Manuscript Received March 21, 2007

First-principles calculations, based on density functional theory, are exploited to investigate the mechanisms and energetics of proton mobility in $CaZrO_3$. The computations accurately reproduce the observed orthorhombic crystal structure of the material. Proton binding sites in the lattice are determined for a range of In dopant concentrations and the corresponding binding strengths are given on a relative energy scale. A proton is typically found to be more strongly bound by 0.1−0.2 eV to the sites at In octahedra than to equivalent sites far from the dopant, though binding energies for certain sites remote from the dopant can exceed those on adjacent octahedra. This suggests that dopant-proton trapping is relatively weak and short-ranged. A series of constrained optimizations is carried out to evaluate minimum-energy paths between the binding sites. A set of proton-transfer jumps and reorientations is identified and associated energy barriers for these proton steps are calculated. It is found that interoxygen transfer and rotation of the proton about a single oxygen have comparable barrier heights. The calculated lowest-energy paths that lead to proton propagation in $CaZrO_3$ exhibit energy barriers in excess of 0.6 eV. Lattice dynamics calculations are used to evaluate the normal modes relevant for proton mobility and the associated attempt frequencies. In this manner, a comprehensive set of data is provided from which the rates of proton migration in In:$CaZrO_3$ may be determined.

I. Introduction

Since the first systematic investigation of high-temperature proton conductivity in ceramic oxides with an ABO_3 perovskite structure,[1] these materials have attracted considerable interest. They have demonstrated potential for use in a range of emerging technologies such as fuel cells,[2] hydrogen pumps,[3] hydrogen separators,[4] steam electrolyzers and steam pumps,[5] humidifiers and dehumidifiers,[6] membrane reactors for hydrogenation and dehydrogenation of hydrocarbons,[7] and sensors (for a recent review, see ref 8). Despite the early promise, the successful application of proton conducting oxides is still facing many technological challenges.[9] A key obstacle to the commercialization of this technology is the high operating temperature and related limitations on the choice of suitable materials. As a result, the only commercialized product to date in the field of proton-conducting ceramics is a hydrogen sensor for molten alumina.[10,11] It is based on $CaZrO_3$ as the electrolyte, doped by In at low concentrations to partially substitute for the higher valent Zr ion and thus enable proton dissolution. Thermochemical stability and a rather low conductivity make this material appropriate for use in low drain applications, such as high-temperature sensors.

The nature of proton migration in zirconates has been studied experimentally,[12] but microscopic details have not yet been fully elucidated. Computer simulations of proton transport usually correlate quite well with experiments, thus providing a complementary insight into the mechanisms of mobility.[13,14] In general, results from various experiments and simulations can lead to rather conflicting interpretations regarding the rate-limiting steps in perovskites.[15] Prior quantum simulation studies of proton migration in $CaZrO_3$[16−18] have been incomplete because of the associated computational cost and have been restricted to the study of only three pathways of proton jumps and the effect of different dopants to proton trapping. In contrast, in the present computational study, a comprehensive set of proton binding sites, jumps, and reorientations in In:$CaZrO_3$ has been investigated, applicable to a range of dopant concentrations. The present paper reports on these processes, their activation energies,

* Corresponding author. E-mail: ante@ivec.org.

(1) Takashi, T.; Iwahara, H. *Rev. Chim. Miner.* **1980**, *17*, 243.
(2) Iwahara, H.; Uchida, H.; Tanaka, S. *Solid State Ionics* **1983**, *9/10*, 1021.
(3) Iwahara, H.; Esaka, T.; Uchida, H.; Yamauchi, T.; Ogaki, K. *Solid State Ionics* **1986**, *18/19*, 1003.
(4) Iwahara, H. *Solid State Ionics* **1999**, *125*, 271.
(5) Iwahara, H.; Hibino, T.; Sunano, T. *J. Appl. Electrochem.* **1996**, *26*, 829.
(6) Iwahara, H.; Matsumoto, H.; Takeuchi, K. *Solid State Ionics* **2000**, *136*, 133.
(7) Hamakawa, S.; Hibino, T.; Iwahara, H. *J. Electrochem. Soc.* **1994**, *141*, 1720.
(8) Iwahara, H.; Asakura, Y.; Katahira, K.; Tanaka, M. *Solid State Ionics* **2004**, *168*, 299.
(9) Iwahara, H. *Solid State Ionics* **1995**, *77*, 289.
(10) Yajima, T.; Koide, K.; Fukatsu, N.; Ohashi, T.; Iwahara, H. *Sens. Actuators, B* **1993**, *13−14*, 697.
(11) Yajima, T.; Koide, K.; Takai, H.; Fukatsu, N.; Iwahara, H. *Solid State Ionics* **1995**, *79*, 333.
(12) Iwahara, H.; Yajima, T.; Hibino, T.; Ozaki, K.; Suzuki, H. *Solid State Ionics* **1993**, *61*, 65.
(13) Kreuer, K. D. *Annu. Rev. Mater. Res.* **2003**, *33*, 333.
(14) Kreuer, K. D.; Paddison, S. J.; Spohr, E.; Schuster, M. *Chem. Rev.* **2004**, *104*, 4637.
(15) Gomez, M. A.; Griffin, M. A.; Jindal, S.; Rule, K. D.; Cooper, V. R. *J. Chem. Phys.* **2005**, *123*, 094703.
(16) Islam, M. S.; Davies, R. A.; Gale, J. D. *Chem. Commun.* **2001**, 661.
(17) Islam, M. S.; Davies, R. A.; Gale, J. D. *Chem. Mater.* **2001**, *13*, 2049.
(18) Islam, M. S. *Solid State Ionics* **2002**, *154−155*, 75.

10.1021/cm070291b CCC: $37.00
Published on Web 05/02/2007

and prefactors, effectively providing for the first time estimates of the rates for a host of individual proton-migration steps. We find a wide range of activation barriers for both proton hops and reorientations, though typical values for both types of motion are comparable. Thus the rate-limiting step cannot be distinguished as being either a single proton jump or rotation, but rather comprises a combination of both types of motion.

II. Computational Methodology

Here, we report a quantum mechanical investigation of proton mobility in $CaZrO_3$ based on density functional theory (DFT). The DFT computations were conducted using the SIESTA methodology and package.[19,20] In this methodology, a linear combination of atomic orbitals (LCAO) is used to expand the Kohn−Sham wavefunctions. Nuclei and core electrons are replaced by norm-conserving pseudopotentials in fully separable form.[21] The scheme of Troullier and Martins[22] was exploited to generate the pseudopotentials, with scalar relativistic corrections included for calcium, zirconium, and indium. The reference atomic valence configurations for the construction of the pseudopotentials were the following: H $1s^1$, O $2s^22p^4$, Ca $3s^23p^64s^2$, Zr $4s^24p^64d^25s^2$, and In $4d^{10}5s^25p^1$. The inclusion of the semicore electrons, i.e., 3s and 3p of Ca, the 4s and 4p of Zr, as well as the 4d of In, is needed because of the sizable overlap of these shells with the conventional valence states.

For electron−electron exchange and correlation interactions, the PBE functional,[23] a form of generalized gradient approximation (GGA), was used for both pseudopotential generation and in the SIESTA calculations. The one-electron Kohn−Sham eigenstates were expanded on a basis of strictly localized[24] numerical pseudo-atomic orbitals.[25] Basis functions were obtained by finding the eigenfunctions of the isolated atoms enclosed within a soft confined spherical potential.[25] A split valence scheme was used to generate a single-ζ basis for the semicore states of Ca, Zr, and In, and a double-ζ basis for the valence states of all the atoms. For oxygen and hydrogen, polarization functions were included, whereas for Zr and Ca, the lowest-lying unoccupied p state was added to the basis set. The optimized basis sets for H, Ca, and O were downloaded from http://www.eminerals.org. The Zr basis set was obtained by a variational energy optimization in cubic bulk ZrO_2, whereas the In basis set was optimized in the bulk In_2O_3 with a bixbyite structure using a simplex search to minimize the total energy.

An auxiliary real space mesh was used to evaluate terms involving the charge density. An equivalent plane-wave cutoff of 350 Ry was used to represent the density. The integrals in reciprocal space were found to be well-converged using in all cases an equivalent cutoff length[26] of 10 Å. This effectively produces a Brillouin-zone sampling of the same quality as a $4 \times 4 \times 3$ Monkhorst−Pack grid for a single crystallographic cell of $CaZrO_3$.

For the description of the calcium zirconate crystal structure, an orthorhombic cell containing four molecular units (i.e., a total of 20 atoms) was used. Calculations for undoped $CaZrO_3$ with the proton employed the same unit-cell geometry as for the pure bulk, with an additional hydrogen atom. However, the total number of electrons in the system was constrained to that of the unprotonated bulk. The charge neutrality of the system was maintained by effectively superimposing a homogeneous negative background.[27] Calculations for In-doped $CaZrO_3$ utilized cell geometries of a size that corresponds to either a $(2 \times 2 \times 1)$ or $(2 \times 2 \times 2)$ supercell of the conventional bulk unit cell, with a single In atom as a substitutional point defect in place of a Zr atom and an additional interstitial hydrogen atom. All the atomic geometries were relaxed via the action of a conjugate gradient optimization procedure until the forces were below 5 meV $Å^{-1}$. For the case of bulk $CaZrO_3$, the unit cell was fully relaxed and subsequently held fixed for the calculations on the doped material.

The energies of the transition states that define kinetic barriers to classically allowed proton transfer were calculated using the "drag" or "reaction coordinate" method. In this simple approach, the minimum energy path (MEP) of a reaction is evaluated by approximating the reaction coordinate by a single degree of freedom, which is varied in steps between the initial and final configurations, and at every step, all other degrees of freedom are optimized. In the present work, the distance of the proton from the coordinating oxygen atom was used as the coordinate for proton translation, whereas the angles that define the direction of the O−H bond were used as the coordinates for proton rotation. This exploits the recently implemented facility to specify the geometry on the basis of a hybrid Z-matrix/Cartesian scheme.[28] The search for the saddle points was subsequently refined by fitting a parabola through three points around each maximum along the MEP. The point along the reaction coordinate at which the parabola reached its maximum value was subsequently tested through a single point energy calculation. In all cases, it was confirmed to be the point of the maximum energy within those sampled from the MEP and therefore it was taken as the transition state.

The vibrational frequencies for stationary points associated with proton diffusion were evaluated within the harmonic approximation. The force constant matrix of each system was determined through central finite differences of the analytic first derivatives by displacing each atom along the three orthogonal Cartesian directions. The eigenvectors and eigenvalues of this matrix define the vibrational normal modes and the associated frequencies. To reduce the computational effort in the case of the large In-doped cell, the full normal mode problem was not solved for all the atoms, but rather only for the O−H−O subgroup that was involved in the proton transfer.

For all proton equilibrium positions, the attempt frequencies for migration were obtained from the comparison of the vibrational Γ-point spectrum of the pure calcium zirconate and that of the protonated counterpart. Namely, in the harmonic approximation to transition-state theory,[29] it is assumed that the phonon modes are harmonic, and this also applies to the modes orthogonal to the reaction coordinate at the saddle points. The rates in this approximation then comprise a prefactor, which is the product of the normal-mode frequencies at the minimum over the product of the non-imaginary modes at the saddle point, and the Boltzmann probability of being at the transition state

$$k = \frac{\prod_i^{3N} \nu_i^{\min}}{\prod_i^{3N-1} \nu_i^{\text{saddle}}} \exp(-\Delta E/k_B T) \qquad (1)$$

(19) Sánchez-Portal, D.; Ordejón, P.; Artacho, E.; Soler, J. M. *Int. J. Quantum Chem.* **1997**, *65*, 453.
(20) Soler, J. M.; Artacho, E.; Gale, J. D.; García, A.; Junquera, J.; Ordejón, P.; Sánchez-Portal, D. *J. Phys.: Condens. Matter* **2002**, *14*, 2745.
(21) Kleinman, L.; Bylander, D. M. *Phys. Rev. Lett.* **1982**, *48*, 1425.
(22) Troullier, N.; Martins, J. L. *Phys. Rev. B* **1991**, *43*, 1993.
(23) Perdew, J. P.; Burke, K.; Ernzerhof, M. *Phys. Rev. Lett.* **1996**, *77*, 3865.
(24) Sankey, O. F.; Niklewski, D. J. *Phys. Rev. B* **1989**, *40*, 3979.
(25) Junquera, J.; Paz, Ó.; Sánchez-Portal, D.; Artacho, E. *Phys. Rev. B* **2001**, *64*, 235111.
(26) Moreno, J.; Soler, J. M. *Phys. Rev. B* **1992**, *45*, 13891.

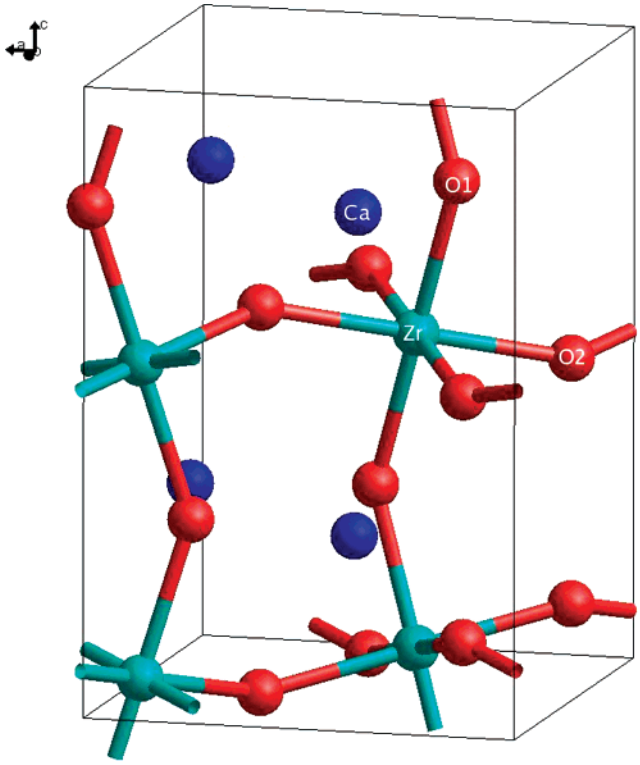

Figure 1. Unit cell of $CaZrO_3$.

where ΔE corresponds to the activation energy, i.e., the energy difference between the saddle point and the minimum. Assuming that the nonimaginary frequencies at the two stationary points mutually cancel out, what is left as the prefactor is a single frequency. It corresponds to the vibrational mode of the proton at the minimum that has the largest projection along the reaction coordinate. Hence, the modes relevant for proton transfer were identified by a visual inspection of the eigenvectors, which represent relative atomic displacements away from the equilibrium sites, using the GDIS package.[30]

III. Results

A. Bulk $CaZrO_3$ Geometry. It is essential that the computational methodology used predicts the known properties of the bulk $CaZrO_3$ prior to the introduction of the dopant and proton. Calcium zirconate crystallizes in the orthorhombic perovskite structure that belongs to the *Pbnm* space group. The structure comprises a three-dimensional framework of corner-linked ZrO_6 octahedra with the divalent Ca cations in a 12-fold coordinated site. The orthorhombic phase, shown in Figure 1, exhibits sizable tilting of the octahedra away from the perfect cubic perovskite configuration, and two distinct oxygen sites, termed apical (O1) and equatorial (O2). The calculated structural parameters, i.e., unit-cell lengths, bond lengths, and bond angles, are given in Table 1 together with their experimental counterparts. The comparison of the values shows reasonable agreement between the observed and simulated crystal structure, with the calculated cell-length parameters slightly exceeding those from experiment, as would be expected from the systematic errors of the GGA. Previous first principles results for the bulk material[16,17] yielded smaller errors for the cell parameters, though this was a due to the cancellation of systematic errors between the use of the LDA derived pseudopotentials that were available at the time with a GGA functional for the valence electrons. Hence the present results are more consistent with the expected behavior for the PBE functional.

Table 1. Calculated and Observed[45] Structural Parameters of Calcium Zirconate

	calcd	obsd
a	5.6435	5.5912
b	5.8303	5.7616
c	8.1159	8.0171
Zr−O (×6) (Å)	2.126	2.096
Ca−O (×4) (Å)	2.389	2.382
Ca−O (×4) (Å)	2.802	2.762
Ca−O (×4) (Å)	3.566	3.510
∠Zr−O(1)−Zr (deg)	144.74	145.76
∠Zr−O(2)−Zr (deg)	145.49	146.50

B. Proton in In-doped $CaZrO_3$. Proton defects are incorporated in the lattice by water vapor treatment. They are believed to reside there in the form of substitutional hydroxyl ions, OH^-, on oxygen ion sites, which are positively charged with respect to the regular lattice (i.e., $OH_O^{\bullet}$ in the Kröger−Vink notation), rather than as interstitial protons. However, the information about the exact proton environment in the lattice is very difficult to extract by spectroscopic techniques[31] and atomic simulations are frequently utilized to assist in the determination of the proton locations in the crystal.

We have studied equilibrium proton positions in calcium zirconate with indium as the dopant on the zirconium site for a range of different In concentrations. First, to identify the intrinsic proton site preferences in calcium zirconate for the dilute limit of dopant concentration or at a considerable distance apart from a dopant atom, we used the original unit cell with the neutralizing charge background and introduced the hydrogen atom at a number of locations surrounding the O(1) and O(2) sites. After optimization, seven different proton binding sites were found, illustrated in Figure 2. The sites labeled with letters A, B, and C are coordinated by the apical O(1) atom, whereas the sites labeled D, E, F, and G are coordinated by the equatorial O(2) atom. The energies, relative to that of site A, are listed in the bottom row of Table 2. Second, the same set of energy minima was tested and reoptimized in the same cell for the proton at the oxygen sites adjacent to a single In substitutional defect. The purpose was to confirm that the same set of proton binding sites persists around the two corners of the dopant centered octahedron. However, the inclusion of the defect breaks the symmetry of the lattice. This effect manifests through the formation of two slightly different types of O(2) site coordinated by the In atom. Consequently, there are two different sets of proton sites associated with the two types of equatorial O(2) atoms. To distinguish between them, we use a primed notation hereafter: O(2′), also shown in Figure 2, is associated with the corresponding proton sites D′, E′, F′, and G′. Because all of these configurations represent an excessive 25% dopant level the respective energies are not

(27) Leslie, M.; Gillan, M. J. *J. Phys. Solid State Phys.* **1985**, *18*, 973.
(28) Hoft, R. C.; Gale, J. D.; Ford, M. J. *Mol. Simul.* **2006**, *32*, 593.
(29) Vineyard, G. H. *J. Phys. Chem. Solids* **1957**, *3*, 121.
(30) Fleming, S. D.; Rohl, A. L. *Z. Kristallogr.* **2005**, *220*, 580.
(31) Nowick, A. S.; Du, Y. *Solid State Ionics* **1995**, *77*, 137.

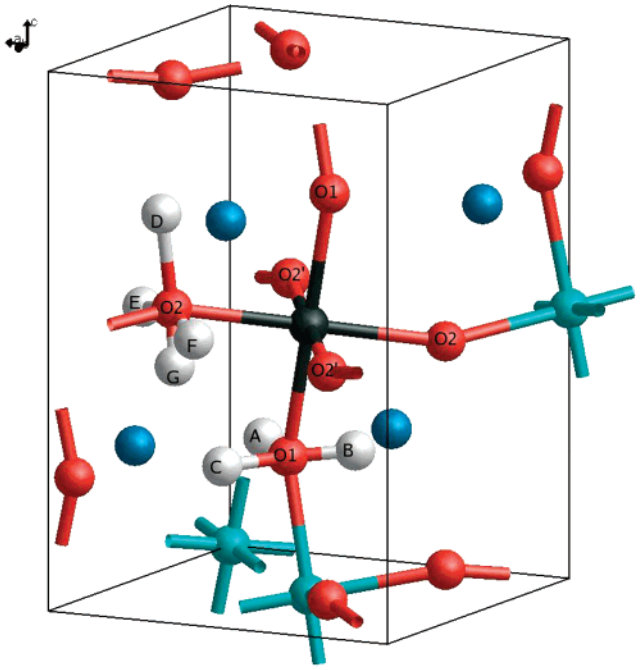

Figure 2. Proton binding sites around the apical O(1) and equatorial O(2) atom in $CaZrO_3$. Here, only one proton-binding site of each type is illustrated for clarity, with the other sites being related by symmetry. Note that when the atom in the center of the octahedra is In, the symmetry is broken and thus O(2) and O(2′) exhibit different binding sites.

provided here. Third, a larger ($2 \times 2 \times 1$) supercell with a single In atom was exploited to test these minima at the O(1) and O(2) sites coordinating the In impurity, which corresponds to a low to moderate dopant concentration of 6.25%. The energies of the sites within this supercell relative to that of the proton at a site A that is at a great distance from the In dopant, are given in the first row of Table 2.

The common feature indicated by the two sets of values in the first and last row of Table 2 is the existence of four strongly binding proton sites, namely A, C, D(D′), and E(E′). The other three binding sites, i.e., B, F, and G(G′), are substantially higher in energy (the F′ site turns out to be nonexistent because the small barrier, discussed in the following subsection, that separates F-type sites from G-type sites is here completely removed and the result is the collapse of F′ to G′). This observation, that B, F, G, and G′ are higher in energy, is generally true regardless of the atom (Zr or In) at the center of the two corner-sharing octahedra.

The two sets of data at the top and the bottom of Table 2 thus provide reference energies for proton binding sites in the lattice in the immediate vicinity of In dopants and at sizable distances from such defects. However, they do not comprise a full list of all the distinct possibilities. That is, because of the presence of the negatively charged defect, a proton at Zr coordinated sites in the vicinity of the In octahedron can have a rather different energy from the proton when it is bound to the same type of site far apart from the dopant, and therefore they need to be taken into account separately. For the characterization of such intermediate binding sites, two different supercells were used. First, the ($2 \times 2 \times 1$) cell was used to evaluate the relative binding energies of those sites that are situated at the Zr-centered octahedra in the *ab* plane around the dopant (in other words, sharing the equatorial corners with the In-centered octahedron). Four apical and four equatorial kinds of O atoms were each found to contribute to a set of A−C and D−G binding sites, respectively. They are accordingly denoted A_i, B_i, ..., G_i, where $i = 1, 2, 3, 4$, as illustrated in Figure 3. A ($2 \times 2 \times 2$) supercell with a single In atom, which corresponds to a low dopant concentration, was exploited to evaluate the energies of the proton binding sites at the Zr centered octahedra along the *c* axis from the dopant (or, in other words, sharing the apical corners with the In-centered octahedron). Four distinct equatorial O atoms were found to contribute to a set of D−G binding sites, denoted D_i, E_i, F_i, and G_i, where $i = 5, 6, 7, 8$, and shown in Figure 3 (note that three out of the four F_i sites collapse to the corresponding G type sites). The binding energies of the intermediate sites, relative to that of the proton at an A site far from the dopant, are given by the eight rows indexed by *i*, where $i = 1, ..., 8$, in Table 2.

By comparing the relative values in Table 2, two observations become evident. First, the energies for the proton coordinated to an In-centered octahedron, shown in the first row, are lower than their counterparts for the proton far apart from the dopant by 100−200 meV, shown in the last row. This attraction to the dopant is clearly a result of the coulomb interaction between the proton and the dopant, and is consistent with previous estimates of the proton trapping energy.[17] Second, the energies of the intermediate states, when the proton is coordinated to a Zr centered octahedron next to the dopant, although on average are close to the values for the dilute limit, exhibit rather large variations of ∼100 meV across the C, D, and E type binding sites. It is also interesting to note that the binding strengths corresponding to the proton in the In-free environment in most cases exceed (i.e., the energies are more negative) their counterparts for the proton at an octahedron adjacent to the dopant. This suggests that coulomb effects are short ranged and often may be overcome by covalent interactions.

To probe the coulomb interactions within calcium zirconate, we have computed the Born effective charge tensors[32] for atoms within selected systems. Here, the Born effective charges are given by

$$q_i^{\mathrm{Born}} = \frac{\partial P^{\alpha}}{\partial \beta_i}$$

where P^{α} is the polarization in the Cartesian direction α. Note that although the absolute polarization is ill-defined, the derivative of this quantity can be determined by finite differences. Because of the orthorhombic system, it is simplest to focus on the diagonalized tensor to place the charges in a unique frame of reference. For the undoped bulk material, the Born effective charges for both Ca and Zr are relatively isotropic with values of +2.40 and +6.57, respectively, with the largest deviation from the mean being less that 0.2 of an electron in both cases. Both the apical and equatorial oxygen ions have Born effective charges of −2.1 orthogonal to the vector between their nearest Zr neighbors,

(32) Baroni, S.; de Gironcoli, S.; Dal Corso, A.; Giannozzi, P. *Rev. Mod. Phys.* **2001**, *73*, 515−562.

Table 2. Energies of the Proton Binding Sites in In:$CaZrO_3$, Relative to the Energy of the A Site in the Dopant Zero Concentration Limit, Given in eV (M is the atom in the octahedral center)

[In] (%)	M−OH−M [*i*]	A	B	C	D(D′)	E(E′)	F(F′)	G(G′)
6.25	In−OH−Zr	−0.184	0.376	−0.130	−0.126(−0.097)	−0.109(−0.090)	0.179(G′	0.158(0.129)
6.25	Zr−OH−Zr [1]	−0.001	0.567	0.016	0.067	0	0.311	0.312
6.25	Zr−OH−Zr [2]	0.006	0.576	−0.025	0.046	−0.018	0.305	0.285
6.25	Zr−OH−Zr [3]	0.001	0.623	0.075	0.048	0.003	0.257	0.285
6.25	Zr−OH−Zr [4]	0.007	0.603	0.066	0.022	−0.018	0.296	0.281
3.125	Zr−OH−Zr [5]				0.013	0.085	G	0.288
3.125	Zr−OH−Zr [6]				−0.020	0.041	0.350	0.312
3.125	Zr−OH−Zr [7]				0.003	0.032	G	0.225
3.125	Zr−OH−Zr [8]				0.027	0.070	G	0.304
0	Zr−OH−Zr	0	0.551	0.008	0.065	0.026	0.332	0.364

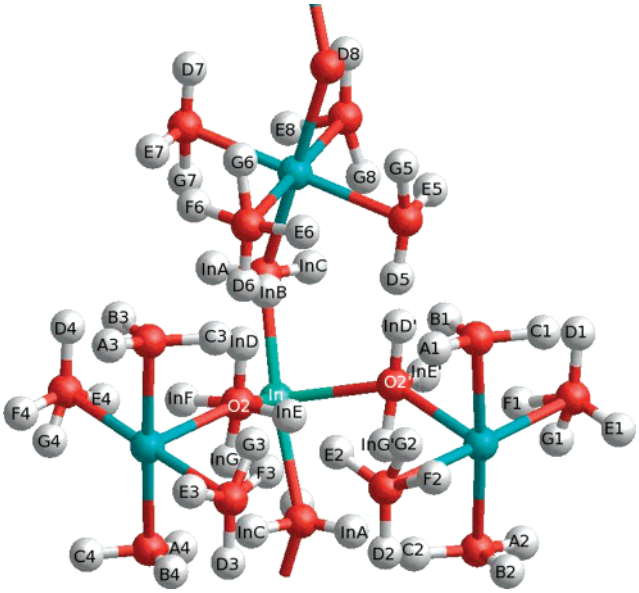

Figure 3. Proton binding sites on the In-centered octahedron and octahedra adjacent to it.

close to the expected ionic state for an oxide ion. However, parallel to the vector between the bonded octahedral cations, the effective charge is much larger with values of −4.66 and −4.80 for the apical and equatorial oxygens, respectively. This higher charge screens the Zr−Zr interaction between neighboring octahedra and results from a directional Zr−O bonding interaction.

On introduction of an indium dopant and charge compensating proton at the low-energy A cation site, the Born effective charge tensor for In is also found to be isotropic with a mean value of +3.76. In contrast, the proton exhibits close to its formal charge (+1.16) along the direction of the hydroxyl bond, whereas it has a significantly lower value of +0.27, on average, at right angles to this. On the basis of the above values, there might be expected to be a large coulomb binding between the indium and proton, given that in a simple monopole representation, the dopant has a charge of almost three electrons less than the zirconium it replaces. However, this is inconsistent with the much weaker binding found by direct calculation and is due to the strong changes in the charge distributions of the surrounding oxygens induced by the presence of indium.

C. Proton Mobility Mechanisms and Energetics. To gain insight into the proton mobility, quantitative information is required about the processes that govern migration. Proton motion in the perovskites is characterized by transfer between adjacent oxygen sites and rotational diffusion around them.[13] We have performed a series of constrained optimizations to evaluate the potential energy profile along linear and angular reaction coordinates. From such MEPs, energy barriers to proton transport have been calculated.

Through the stepwise variation of the distance between H and coordinating O atoms a number of possible proton-transfer processes between distinct oxygen atoms have been identified. They are listed in Table 3 along with the associated energy barriers. The first column in Table 3 refers to the proton jumps from the binding sites on the In-centered octahedron. The second, third, and fourth columns comprise the transfer processes for which the initial configuration is one of the intermediate binding sites, that is A_i, B_i, C_i, where $i = 1, 2, 3, 4$; D_i, E_i, F_i, G_i, where $i = 1, 2, 3, 4$; and D_i, E_i, F_i, G_i, where $i = 5, 6, 7, 8$, respectively. The transfer mechanisms that involve initial and final configurations in which the proton is far from a dopant atom for both cases are listed in the fifth column. Finally, the sixth column shows the proton hops and corresponding energy barriers for which the proton in the initial conformation is just outside of the range of interaction with a dopant, but the final conformation is one of the intermediate binding sites.

It is interesting to compare these results with available counterparts from a previous computational work[17] on the same system: there, the two barriers for the interoctahedral and intraoctahedral proton jumps, which correspond to A → C and A → G processes, were evaluated to be 0.14 and 0.58 eV, respectively. These differ from the values 0.210 and 0.644 eV obtained in the present work by 65−70 meV, but the difference between the two barrier heights is consistent: 0.44 eV in the previous work vs 0.434 eV in the current work. The higher barriers found in the present study can be attributed to a more refined procedure for the identification of transition states, as well as the slightly larger lattice parameters, which results in greater O−H distances at the saddle points. The values of the two activation energies are illustrative of a more general trend. As Table 3 shows, the barriers to proton hops are mostly in the 0.1−0.2 eV range when the final configuration involves the proton in one of the low energy states, that is type A, C, D, and E binding sites. On the other hand, if the final configuration is one of the high-energy states (that is, B, F, or G type proton binding sites), the barrier is in excess of 0.5 eV.

By the stepwise variation in the orientation of the O−H bond, energy barriers to proton diffusional rotation around the coordinating oxygen atom have been evaluated. In the case of apical O atoms, the obvious choice for the frozen coordinate was the azimuthal angle, whereas in the case of

Table 3. Activation Energy, ΔE, for Proton Hop between the Initial (i) and Final State (f) Given in eV

i	f	ΔE	i	f	ΔE	i	f	ΔE	i	f	ΔE	i	f	ΔE	i	f	ΔE
In A	In G′	0.534	A_1	G_2	0.588	D_1	D	0.118	D_5	In D′	0.036	A	C	0.210	A	C_1	0.177
In A	C_2	0.256	A_1	C	0.205	E_1	E	0.131	E_5	E	0.147	A	G	0.644	A	C_3	0.263
In A	G_7	0.609	B_1	In D′	0.136	F_1	In E′	0.256	G_5	A	0.282	B	D	0.201	A	C_4	0.257
In B	In D	0.182	C_1	A	0.161	G_1	A_2	0.278	D_6	In D	0.037	C	A	0.202	A	G_3	0.594
In C	A_4	0.273	A_2	G_1	0.584	D_2	D	0.110	E_6	E	0.141	D	B	0.688	A	G_4	0.601
In D	In B	0.685	A_2	C	0.228	E_2	In E	0.073	F_6	E_7	0.317	D	D	0.119	A	G_5	0.570
In D	D_6	0.143	B_2	D	0.186	F_2	E	0.277	G_6	A	0.271	E	E	0.202	A	G_6	0.583
In E	E_2	0.171	C_2	In A	0.098	G_2	A_1	0.302	D_7	D	0.100	E	F	0.549	C	A_1	0.196
In E	F_3	0.561	A_3	C	0.200	D_3	D	0.115	E_7	F_6	0.635	F	E	0.243	C	A_2	0.226
In F	In E′	0.303	B_3	D	0.196	E_3	E	0.123	E_7	E	0.140	G	A	0.280	C	A_3	0.193
In G	A_4	0.409	C_3	A	0.188	F_3	In E	0.195	G_7	In A	0.200				D	B_2	0.697
In D′	B_1	0.799	A_4	In C	0.136	G_3	A	0.309	D_8	D	0.104				D	B_3	0.754
In D′	D_5	0.146	A_4	In G	0.560	D_4	D	0.107	E_8	E	0.151				D	B_4	0.730
In E′	In F	0.572	A_4	G_8	0.620	E_4	In E′	0.074	G_8	A_4	0.323				D	D_1	0.120
In E′	F_1	0.658	B_4	D	0.192	F_4	E	0.302							D	D_2	0.091
In E′	E_4	0.154	C_4	A	0.191	G_4	A	0.320							D	D_3	0.098
In G′	In A	0.221													D	D_4	0.064
															D	D_7	0.038
															D	D_8	0.066
															E	E_1	0.105
															E	F_2	0.556
															E	E_3	0.100
															E	F_4	0.572
															E	E_5	0.206
															E	E_6	0.156
															E	E_7	0.146
															E	E_8	0.195

Table 4. Activation Energy, ΔE, for Proton Reorientations between the Initial (i) and Final State (f) Given in eV

i	f	ΔE	i	f	ΔE	i	f	ΔE	i	f	ΔE	i	f	ΔE
In A	In B	0.844	C_1	A_1	0.854	F_1	D_1	0.127	F_4	D_4	0.217	D_8	E_8	0.516
In A	In C	0.802	C_1	B_1	0.588	F_1	E_1	0.033	F_4	G_4	0.013	D_8	G_8	0.537
In B	In A	0.283	A_2	B_2	0.831	G_1	E_1	0.150	G_4	E_4	0.150	E_8	D_8	0.472
In B	In C	0.017	A_2	C_2	0.799	G_1	F_1	0.032	G_4	F_4	0.028	E_8	G_8	0.342
In C	In A	0.748	B_2	A_2	0.261	D_2	E_2	0.469	D_5	E_5	0.515	G_8	D_8	0.260
In C	In B	0.524	B_2	C_2	0.038	D_2	F_2	0.480	D_5	G_5	0.544	G_8	E_8	0.109
In D	In E	0.545	C_2	A_2	0.830	E_2	D_2	0.532	E_5	D_5	0.442	A	B	0.695
In D	In F	0.492	C_2	B_2	0.640	E_2	G_2	0.454	E_5	G_5	0.370	A	C	0.861
In E	In D	0.528	A_3	B_3	0.898	F_2	D_2	0.222	G_5	D_5	0.269	B	A	0.143
In E	In G	0.370	A_3	C_3	0.918	F_2	G_2	0.011	G_5	E_5	0.168	B	C	0.061
In F	In D	0.187	B_3	A_3	0.276	G_2	E_2	0.152	D_6	E_6	0.603	C	A	0.853
In F	In G	0.013	B_3	C_3	0.011	G_2	F_2	0.030	D_6	F_6	0.507	C	B	0.604
In G	In E	0.102	C_3	A_3	0.840	D_3	E_3	0.452	E_6	D_6	0.542	D	E	0.477
In G	In F	0.034	C_3	B_3	0.560	D_3	F_3	0.482	E_6	G_6	0.407	D	F	0.477
In D′	In E′	0.558	A_4	B_4	0.851	E_3	D_3	0.496	F_6	D_6	0.137	E	D	0.515
In D′	In G′	0.470	A_4	C_4	0.894	E_3	G_3	0.443	F_6	G_6	0.018	E	G	0.419
In E′	In D′	0.552	B_4	A_4	0.255	F_3	D_3	0.273	G_6	E_6	0.136	F	D	0.210
In E′	In G′	0.382	B_4	C_4	0.028	F_3	G_3	0.034	G_6	F_6	0.056	F	G	0.051
In G′	In D′	0.244	C_4	A_4	0.835	G_3	E_3	0.161	D_7	E_7	0.532	G	E	0.081
In G′	In E′	0.163	C_4	B_4	0.565	G_3	F_3	0.006	D_7	G_7	0.557	G	F	0.019
A_1	B_1	0.835	D_1	E_1	0.476	D_4	E_4	0.518	E_7	D_7	0.503			
A_1	C_1	0.871	D_1	F_1	0.371	D_4	F_4	0.492	E_7	G_7	0.346			
B_1	A_1	0.267	E_1	D_1	0.543	E_4	D_4	0.558	G_7	D_7	0.337			
B_1	C_1	0.037	E_1	G_1	0.462	E_4	G_4	0.449	G_7	E_7	0.153			

equatorial O atoms, the reaction coordinate was approximated by the polar angle. The barriers for A−B−C and D−E−(F−)G proton rotations are given in Table 4. They are listed in the order starting from the sites on the In-centered octahedron, followed by those that are part of its nearest neighboring octahedra, down to the sites on Zr-centered octahedra far from the dopant.

In the case of rotations around the apical O atoms, regardless of the cation at the octahedron center, the common features are (i) very high barriers, in excess of 0.8 eV, separating the A site from both the high-energy B site and low-energy C site; (ii) very low barriers, of several tens of millielectron volts, for the rotation from the B to C site; (iii) moderate barriers, of 0.15−0.3 eV, for the rotation from the B to A site; and (iv) rather high barriers, of 0.5−0.8 eV, that separate the C site from the other two. The rotation around equatorial O atoms is characterized by (i) substantial barriers of ∼0.5 eV separating the D site from both the low-energy E site and high-energy F site (G site in some cases), (ii) similarly sized barriers between the E site and G site, (iii) tiny (if any) barriers for the motion from the G site to the F site and vice versa, and (iv) moderate 0.15−0.3 eV barriers that separate the F site (G in some cases) from the D site.

Molecular dynamics simulations of protons in cubic $BaCeO_3$,[33] $BaZrO_3$ and $BaTiO_3$[34] perovskites, employing

(33) Münch, W.; Seifert, G.; Kreuer, K. D.; Maier, J. *Solid State Ionics* **1996**, *86−88*, 647.
(34) Münch, W.; Seifert, G.; Kreuer, K. D.; Maier, J. *Solid State Ionics* **1997**, *97*, 39.

forces from electronic structure methods, have revealed rapid reorientation of hydroxyl ions around the M−OH bond (M = Ce, Zr, Ti) on a time scale of 1×10^{-12} s for a complete proton rotation around the O atom. In contrast, proton jumps in $BaCeO_3$ are observed[35] only over a time on the order of magnitude of 1×10^{-9} s. On the basis of these results, it has been frequently suggested[13,36,37] that the reorientation is facile and characterized by low activation barriers, whereas the proton transfer is rare and thus the rate-limiting step. In fact, experimental activation energies of ~0.1 eV have been reported[38] for proton rotations around the coordinating oxygen atom in a related quaternary perovskite type oxide. The results in Tables 3 and 4 portray a rather different picture of proton diffusivity in the highly distorted $CaZrO_3$ perovskite. Here, we observe a wide range of barrier heights for both proton hops and rotations. Hence, neither can be obviously singled out as the rate-limiting step.

It is interesting to note that the lowest-energy paths that start from one of the favorable binding sites, e.g., A, C, D, or E in the zero In concentration limit, do not actually lead to the propagation of proton through the crystal; for all four sites, the lowest-energy path is simply an interoctahedral exchange of proton back and forth, i.e., A ↔ C, D ↔ D, and E ↔ E. Even for a proton that starts out from a high-energy site, such as B, F, or G, a similar scenario applies because the proton easily finds its way to a low-energy intraoctahedral counterpart, that is D, E, and A via hopping, or C, D, and E via rotation, respectively (by neglecting the almost barrierless rotations F ↔ G). Hence, the lowest energy paths that do lead to the proton propagation in $CaZrO_3$ cannot bypass the steps with higher activation energies ranging from 0.4 to 0.9 eV. For example, for a proton starting from an A type site and arriving at the same type of site on another octahedron, the lowest-energy path comprises the following steps: A → C (hop, 0.210 eV), C → B (rotation, 0.604 eV), B → D (hop, 0.201 eV), D → F (rotation, 0.477 eV), F → G (rotation, 0.051 eV), and G → A (hop, 0.280 eV). The highest-energy barrier along this path, which comprises all but E type sites, is 0.604 eV. However, this is not much more than 0.53 eV, recently evaluated for $CaZrO_3$ in a hypothetical cubic lattice.[15] If an analogous MEP is considered starting from an In dopant, i.e., In A → C_2 → B_2 → D, etc., the highest-energy barrier is slightly higher, 0.64 eV. A symmetrical path that includes E type sites is also plausible: A → G (hop, 0.644 eV), G → E (rotation 0.081 eV), E → E (hop, 0.202 eV) E → G (rotation, 0.419 eV), and G → A (hop, 0.280 eV), with a maximum energy of 0.644 eV. Such a path in the vicinity of In would actually have a lower maximum energy, because of either In A → In G′ (hop, 0.534 eV) or A_4 → In G (hop, 0.560 eV).

D. Proton Dynamics in $CaZrO_3$. Molecular dynamics simulations of a proton in $CaZrO_3$[16,17] showed rapid rotational and stretching motions of the hydroxyl group, whereas in the cubic perovskites,[33,34] mostly intraoctahedral proton transfer was observed. In the case of $CaZrO_3$ the simulations predicted predominantly interoctahedral proton jumps,[17] consistent with a lower proton mobility in the orthorhombic perovskites.[36,37] The simulations also demonstrated large variations in the interatomic distance between neighboring O atoms involved in proton exchange, indicating the importance of lattice dynamics and implying that proton transfer is vibration assisted through quasirigid modes.

At relatively low temperatures, proton conductivity exhibits Arrhenius-type behavior.[31,39] Hence, to evaluate rates for the various processes involved in proton motion in $CaZrO_3$, which have been identified in the current study, reasonable estimates of the prefactors (attempt frequencies) are needed in addition to the associated activation energies from Tables 3 and 4. We have determined the prefactors from the vibrational normal mode spectra of the configurations with proton at its binding sites. We assume that the mode frequencies at the minimum and saddle cancel out and what is left as the prefactor is the frequency of the mode in the direction of the reaction coordinate. This assumption has been tested in the case of the transition state for the E → E proton hop. The single-frequency approximation results in a prefactor of 3040 cm^{-1}, whereas the ratio of the two products of the full sets of frequencies at the stationary states gives 2500 cm^{-1}. Given the uncertainties in the activation energies, which are more critical due to the exponential dependence, the error due to the use of the single-frequency approximation is quite acceptable.

To further validate the approach used to determine the prefactor, the phonon spectra of the configurations with the proton in one of seven binding sites far from the dopant (A−G) were first evaluated and compared with that of the pure $CaZrO_3$. The full unit-cell configuration, with a neutralizing background for the protonated structures, was exploited to this end. Because the all-atom normal mode calculations are expensive when a large number of atoms is involved, the spectra were also evaluated for the protonated geometries in the approximation in which only displacements of the hydroxyl ion and the closest O atom are permitted. The purpose of this exercise was twofold. First, from the comparison of the all-atom and O−H−O group spectra, the accuracy of the localized vibration approximation can be ascertained, which is very important for the correct use of the approximation in larger systems. Second, the identification of the modes involved in the mechanisms of proton motion is facilitated by the removal of all but nine modes left in the approximate spectrum.

The calculated spectra are shown in Figure 4. The principal difference between the phonon spectrum of the pure crystal, given on the left, and those of protonated structures is that former displays excitations only in the 0−750 cm^{-1} range, whereas all of the latter exhibit three peaks with distinctly higher frequencies: one at ~3000 cm^{-1} and two in the 750−1400 cm^{-1} range. The three modes can thus be attributed to proton motion, which is largely decoupled from that of the heavier lattice. This assignment is corroborated by the O−H−O group spectra, which all show the three excitations

(35) Kreuer, K. D.; Schönherr, E.; Maier, J. *Solid State Ionics* **1994**, *70−71*, 278.
(36) Kreuer, K. D. *Chem. Mater.* **1996**, *8*, 610.
(37) Kreuer, K. D. *Solid State Ionics* **1999**, *125*, 285.
(38) Pionke, M.; Mono, T.; Schweika, W.; Springer, T.; Schober, H. *Solid State Ionics* **1999**, *125*, 497.
(39) Goodenough, J. B. *Annu. Rev. Mater. Res.* **2003**, *33*, 91.

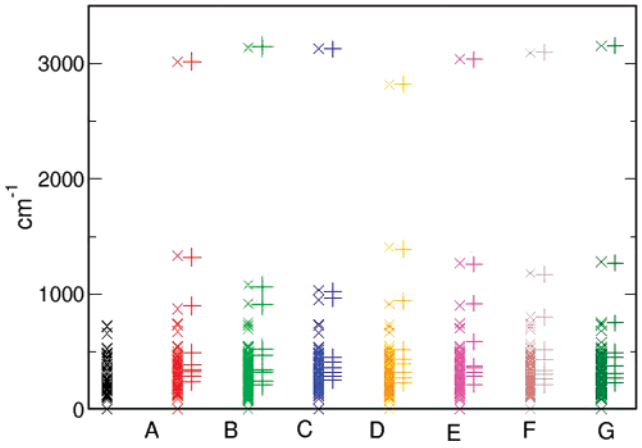

Figure 4. Computed normal-mode frequencies at the Γ-point of the pure $CaZrO_3$ (in the left column) and with a proton at one of the seven binding sites. For the latter, two columns are shown, one that is obtained from the all-atom calculation (symbol ×) and one obtained from the approximate procedure (symbol +) in which only displacements of the hydroxyl ion group and the closest O atom are allowed.

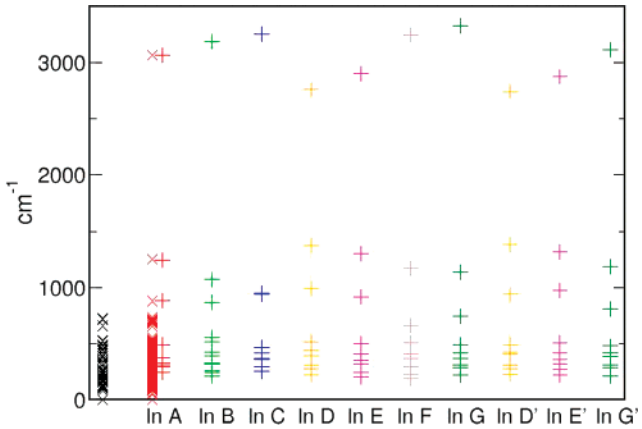

Figure 5. Computed normal-mode frequencies at the Γ-point of $CaZr_{0.9375}In_{0.0625}HO_3$. For comparison, the left column shows is for the pure $CaZrO_3$, whereas the rest are for the doped crystal with the proton at one of the 10 binding sites on the In-centered octehedron. For the In A site, two columns are shown, one that is obtained from the all-atom calculation (symbol ×) and one obtained from the approximate procedure (symbol +) in which only displacements of the hydroxyl ion group and the closest O atom are allowed. For all the others, only the approximate spectrum was evaluated.

at almost identical frequencies to their all-atom counterparts, whereas the other six modes overlap with those of the pure crystal.

In addition to the undoped material, the spectra of the configurations with the proton in one of ten binding sites about the In-centered octahedron were evaluated. The large (2 × 2 × 1) supercell with a single In atom was employed for these calculations. An all-atom calculation was carried out only in one case, that of the proton at the In A binding site, whereas for the rest, the approximate procedure that involves only the O−H−O group was utilized. The calculated spectra are shown in Figure 5. These vibrational spectra are not notably different from those shown in Figure 4. A closer inspection indicates that of the three proton modes, the one with the lowest frequency, in the case of In F and In G configurations, has become degenerate with lattice excitations. This mode softening is simply a consequence of the very low barrier to rotational motion In G ↔ In F (see Table 4), which, in the case of the G′ site, is completely lost.

Table 5. Attempt Frequencies ν for Proton Hop between the Initial (i) and Final State (f) Given in cm^{-1} (in the case of the processes for which the activation energies could not be calculated, the entries are given in parenthesis)

i	f	ν	i	f	ν
In A	In G′	881	A	C	3017
In A	C_2	3067	A	G	896
In A	G_7	881	B	D	3145, 1062
In B	In D	3185, 1074	C	A	3127
In C	A_4	3256	(C)	(G)	(962)
(In C)	(In G)	(949)	D	B	939
In D	In B	987	D	D	2823
In D	D_6	2760	E	E	3040
In E	E_2	2902	E	F	919
In E	F_3	915	F	E	3097, 1170
In F	In E′	3243, 1173	G	A	3158, 1269
In G	A_4	3325, 1136	(G)	(C)	(3158, 1269)
(In G)	(In C)	(3325, 1136)			
In D′	B_1	938			
In D′	D_5	2737			
In E′	In F	977			
In E′	F_1	977			
In E′	E_4	2874			
In G′	In A	3115, 1184			
(In G′)	(C_2)	(3115, 1184)			

The frequencies of the proton vibrations that contribute to proton hopping are given in Table 5. Several observations can be made. First, their frequencies are close either to 1000 or 3000 cm^{-1}. The former correspond to bending modes of the O−H bond around the oxygen atom, whereas the latter are stretching modes of the hydroxyl group. Second, for every initial binding configuration, there are two vibration modes in Table 5. In most cases, they contribute to two different hops. However, in the case of the high-energy initial configurations, that is B, F, and G, although orthogonal, both modes contribute to a proton hop to the same final configuration. The reason for this is simply because the stretching mode at these sites points toward the same type of site on adjacent octahedra. These are rather far apart from the initial sites. Halfway between them are two low-lying sites of either D, E, or A(C) type, respectively, whose basins of attraction would eventually capture the traversing proton, thus preventing a long-range jump. The bending modes at their turning points also point toward these sites, and therefore both the stretching and bending modes possess a projection onto the same proton jump. Hence, to evaluate the associated rates, the appropriate choice of the prefactor for such processes would be a function of the two frequencies. Third, there are no substantial differences between the frequencies for the sites on purely Zr octahedra and those on the In octahedron. This observation is important because it implies that the frequencies for the former can be taken as the prefactor for the hops from the large set of intermediate sites (that is, the sites on the Zr-centered octahedra adjacent to the In-centered octahedron).

The frequencies of the proton modes that contribute to proton rotations are given in Table 6. They correspond to bending modes of the O−H bond orthogonal to the stretching mode and the bending mode that gives rise to proton hopping. Accordingly, the frequencies are on average about 1000 cm^{-1}, although the variations are quite large, ranging from ∼700 cm^{-1} for rotations around the F and G type sites to ∼1300 cm^{-1} for rotations around the A, D, and E type sites. Again, the differences between the frequencies for the sites

Table 6. Attempt Frequencies ν for Proton Reorientations between the Initial (i) and Final State (f) Given in cm^{-1}

i	f	ν	i	f	ν
In A	In B, In C	1244	A	B, C	1319
In B	In A, In C	865	B	A, C	907
In C	In A, In B	949	C	A, B	1027
In D	In E, In F	1375	D	E, F	1392
In E	In D, In G	1304	E	D, G	1260
In F	In D, In G	666	F	D, G	802
In G	In E, In F	742	G	E, F	750
In D′	In E′, In G′	1384			
In E′	In D′, In G′	1314			
In G′	In D′, In E′	812			

on purely Zr octahedra and those on the In octahedron are minor and the former can be taken as the prefactor for the rotations around the binding sites in the vicinity of the In-centered octahedron.

IV. Discussion

The processes described in terms of the binding sites, activation barriers, and attempt frequencies provide a relatively comprehensive sketch of equilibrium protonic mobility in In-doped $CaZrO_3$. Because of the complexity of the distorted perovskite system, it is difficult to go analytically from the tabulation of rates for individual steps to an overall macroscopic diffusion rate for the bulk material. However, the present data can be readily be exploited as part of a kinetic Monte Carlo[40] simulation to determine mobility as a function of indium concentration. This application of the present results is currently underway and will be reported subsequently.

In analyzing the present results, potential limitations of the approach should be discussed. First, not all conceivable proton-transfer mechanisms were located by the constrained optimization reaction-coordinate technique. The majority of the direct intersite pathways that could not be located represent long-range proton hops. Typically, during the search for these transition states, the proton would fall into the basin of attraction for a different minimum. Although it is quite plausible that long-range hops take place by a combination of two or more shorter jumps, it is impossible to be absolutely sure that there is no direct pathway without the use of second-derivative-based techniques, such as rational function optimization,[41] because of the finite step length within the present method. Second, the drag technique, in combination with first-derivative-only optimization, can lose accuracy when there are soft modes present. This can manifest itself through hysteresis or difficulty in minimization of forces in the region of the transition state. The above issues have been particularly problematic during the evaluation of the barriers for D ↔ E, In D ↔ In E, and In D′ ↔ In E′ rotations, respectively, and thus these activation energies, as quoted in Table 4, carry a larger uncertainty than the others. The deficiencies of the method were also acute when we attempted to evaluate the barriers for the long-range proton jumps between C and G type sites. The possibility of such processes was indicated by the normal mode calculations, though this is not a guarantee that a pathway exists should it be highly nonlinear. Despite our best efforts, we could not locate estimates for those barriers, which is why the corresponding attempt frequencies are shown in parenthesis in Table 5 to denote the absence of a related pathway. Nevertheless, in a previous work[17] a barrier of 0.74 eV was ascribed to the C → G proton transfer. Given the high activation energy, the process is likely to be of lesser importance than the others that involve the neighboring A site, namely A ↔ C and A ↔ G, and the proton could propagate between G and C more easily via a two-step process that involves an intermediate A site. Similar scenarios would apply to a range of many other long-range proton jumps that could not be located by the drag technique. Consequently, as long as the short-range hops are described accurately, this is ultimately not a serious deficiency of the methodology.

Arguably, a more serious limitation of the current approach to transition state identification is that only the proton position relative to the coordinating oxygen atoms was considered as the reaction coordinate for diffusion. The problem with this strategy is that it does not explicitly allow for a range of transport processes that are only weakly coupled to the hydroxyl bond length and therefore this might lead to a ill-conditioned reaction coordinate. For instance, a proton can be carried over a considerable distance by a normal mode that involves its coordinating O atom without a great change to the relative proton position. A number of such modes, with frequencies ranging 200−700 cm^{-1}, have been observed in the current work. Some of these modes have an orientation such that they can considerably reduce the O−O separation during vibration and bring the proton into the vicinity of an adjacent O atom, making a temporary hydrogen bond with it. From there, the proton can eventually make a shorter hop on to the other binding site. Such a proton transfer is frequently termed "adiabatic"[36,42] in the sense that no or very little excitation of the proton-transfer coordinate is involved in the process, i.e., the proton remains in its vibrational ground state. Hence, the activation of proton hops can be viewed as that of the host and target oxygen atom, which would also account for the fact that that $CaZrO_3$ exhibits oxide ion conductivity.[12,43] Accurate computation of the prefactors for such modes would require more extensive vibrational calculations for a larger subset of atoms within the surrounding lattice, though it could still be expected that there would be substantial cancellation of modes between the two stationary states. Furthermore, use of Hessian-based methods could overcome the difficulty of precisely locating the transition state through improved preconditioning of the minimization. However, the errors associated with the suboptimal choice of reaction coordinate due to a weakly coupled soft mode will predominantly lie in the transition-state geometry, rather than the estimate of the barrier height. Furthermore, such rigid mode-driven processes are considered to be much more important in the case of good proton conductors such as $BaCeO_3$ and $BaZrO_3$

(40) Voter, A. F. Kinetic Monte Carlo. In *Radiation Effects in Solids*; Sickafus, K. E., Kotomin, E. A., Uberuaga, B. P., Eds.; NATO Science Series; Springer: New York, 2007; Vol. 235.
(41) Banerjee, A.; Adams, N.; Simons, J.; Shepard, R. *J. Phys. Chem.* **1985**, *89*, 52−57.
(42) Kreuer, K. D.; Fuchs, A.; Maier, J. *Solid State Ionics* **1995**, *77*, 157.
(43) Dudek, M.; Bućko, M. M. *Solid State Ionics* **2002**, *157*, 183.

with the simple cubic perovskite structure[13,36,37] than for the modestly conducting $CaZrO_3$ with an orthorhombic structure.

Finally, we make no attempt to investigate the influence of the quantum behavior of the hydrogen nucleus, and in particular the tunneling of proton through the barriers.[44] Tunneling is likely not to be critically important, given the high temperature required for proton conductivity in perovskite type oxides. Even though there is no evidence to suggest that proton tunneling can be ruled out, it is often assumed[36] that in perovskites it is much less important than in metals. Certainly in the "adiabatic" limit one can safely discard the tunneling effects, but they may be substantial for proton rotations with large barriers, such as A ↔ C, and the long-range proton hops with narrow profile barriers, such as C ↔ G.[17] Verification of the importance of hydrogen quantum behavior through path integral molecular dynamics remains a challenge for the future because of the extended timescales required to reliably sample diffusion.

V. Conclusions

Microscopic quantities relevant for proton mobility in $CaZrO_3$ have been determined by nonlocal density functional theory within periodic boundary conditions. This methodology has been found to accurately describe the orthorhombic geometry of the bulk material. Starting from this equilibrium structure, proton binding sites have been identified in the undoped lattice, i.e., at the zero dopant concentration limit. This characterizes the intrinsic site preferences of the proton in the absence of dopant-hydrogen interactions. Subsequently, equilibrium proton positions have been determined for the oxygen sites that are part of the In-centered octahedron and for the sites situated on the set of nearest neighbor Zr octahedra. Thus, a complete energy landscape for the most important proton binding sites in $In:CaZrO_3$ has been generated.

Starting from these local energy minima, a series of constrained optimizations have been conducted to investigate the potential energy profile for proton diffusion between adjacent sites. A large number of possible proton-transfer jumps and rotations have been characterized and the associated energy barriers for these proton steps have been evaluated. Contrary to previous indications, on the basis of studies of limited subsets of the available pathways for diffusion, it is found that both interoxygen transfer and rotation of the proton about a single oxygen have comparable barrier heights in general. Although the activation energy for certain diffusive moves is low, in order to migrate between two periodic images of the same site separated by a lattice vector, it is necessary to encounter a higher barrier at some stage of the pathway. Because of the complex arrangement of pathways, it is hard to directly determine the optimal diffusion direction. However, it appears likely that the lowest barrier for bulk diffusion would be at least 0.6 eV, with an additional barrier in the region of In of 0.04 eV due to dopant-proton trapping.

Lattice dynamics calculations have been carried out to evaluate the normal modes relevant for proton mobility and the associated attempt frequencies. Hence, all the information required to determine the rates of proton migration, within the limits of harmonic transition state theory, have been identified. These rate constants are now being employed within kinetic Monte Carlo simulation in order to identify the likely pathways and overall rates for proton diffusion as a function of indium concentration and distribution.

Acknowledgment. We thank the Australian Research Council for financial support through a Discovery grant. The use of supercomputer facilities at the Australian Partnership for Advanced Computing (APAC) and iVEC is gratefully acknowledged. J.D.G. thanks the Government of Western Australia for the award of a Premier's Research Fellowship.

CM070291B

(44) Matsushita, E.; Tanase, A. *Solid State Ionics* **1997**, *97*, 45.
(45) Koopmans, H. J. A.; van de Velde, G. M. H.; Gellings, P. J. *Acta Crystallogr., Sect. C* **1983**, *39*, 1323.